




Universal fluctuations of global geometrical measurements in planar clusters

Silvia N. Santalla ¹, Ivan Álvarez Domenech ², Daniel Villarrubia ³, Rodolfo Cuerno ³ and Javier Rodríguez-Laguna ⁴

¹*Dto. Física & GISC, Universidad Carlos III de Madrid, Leganés 28911, Spain*

²*Dto. Física Matemática y de Fluidos, Universidad Nacional de Educación a Distancia, Las Rozas 28232, Spain*

³*Dto. Matemáticas & GISC, Universidad Carlos III de Madrid, Leganés 28911, Spain*

⁴*Dto. Física Fundamental, Universidad Nacional de Educación a Distancia, Madrid 28040, Spain*



(Received 2 December 2023; accepted 26 February 2024; published 22 March 2024)

We characterize universal features of the sample-to-sample fluctuations of global geometrical observables, such as the area, width, length, and center-of-mass position, in random growing planar clusters. Our examples are taken from simulations of both continuous and discrete models of kinetically rough interfaces, including several universality classes, such as Kardar-Parisi-Zhang. We mostly focus on the scaling behavior with time of the sample-to-sample deviation for those global magnitudes, but we have also characterized their histograms and correlations.

DOI: [10.1103/PhysRevE.109.034127](https://doi.org/10.1103/PhysRevE.109.034127)

I. INTRODUCTION

Characterizing the statistical properties of rough interfaces away from equilibrium is one of the main tasks in a variety of scientific contexts, such as the growth of solid phases in contact with a vapor [1], liquid-crystal turbulence [2], the shapes of isochrone curves on rough terrains [3,4], the growth of bacterial colonies or cell aggregates [5], or even the shape of a city skyline [6]. One of the most relevant insights was provided by the Family-Vicsek (FV) dynamic scaling ansatz [7], which proposed that the width, or roughness, of a rough interface grows with time t as a power law, $W \sim t^\beta$, where β is called the *growth exponent*, up to a saturation $t_{\text{sat}} \sim L^z$, where z is called the *dynamical exponent* and L is the lateral size of the system. The FV ansatz suggests the existence of a well-defined *correlation length* $\xi \sim t^{1/z}$, such that the roughness at length scales $\ell \ll \xi$ will always be saturated, $w(\ell) \sim \ell^\alpha$, where α is the *local roughness exponent*, and the three exponents are related as $\alpha = \beta z$ within the FV formalism [1,8].

The values of the scaling exponents β and z are typical hallmarks of the kinetic roughening *universality class*. For example, for one-dimensional (1D) interfaces, $\beta = 1/3$ and $z = 3/2$ in the Kardar-Parisi-Zhang (KPZ) universality class [1,8,9], which is associated with growth along the local normal direction combined with surface tension effects and time-dependent noise. Interestingly, the KPZ universality class is able to also fix the one-point and the two-point (correlation) statistics of the local interface or front fluctuations, which are associated with Airy processes of different types, depending on whether the overall symmetry of the growth system is, e.g., flat or circular [2,8,10,11]. Additionally, the statistical properties of global system quantities such as the (squared) roughness W^2 have been characterized in detail for globally flat KPZ interfaces (the case for, e.g., periodic boundary conditions) [8,12,13]. Notably, an equivalent result seems to be lacking for the case of growing two-dimensional clusters, which in general remains somewhat less understood in spite of its large interest for diverse contexts from

epitaxial growth [14] to cellular aggregates [15]. For instance, as clarified in Ref. [16], the additional degrees of freedom implied by the dynamics of 2D clusters (such as the evolution of their center of mass) have sometimes even led to incorrect identification of the exponent values and universality classes for their corresponding 1D fronts. More recently [17], suitable characterizations of the cluster dynamics have been shown to extract correct exponent values and even the detailed time evolution for certain measures of 2D clusters under growth or dissolution conditions.

The aim of the present article is to characterize the global properties defined in each case as a whole for 2D growing clusters. Through a scaling analysis, nontrivial predictions, such as scaling exponent values, will be derived from general considerations on the sample-to-sample fluctuations of such properties. Specifically, we will consider the average radius R , the total area A , the total width W , the (suitably regularized) length L , and the center-of-mass displacement R_{cm} . As we will show, the expected values of these magnitudes and their deviations grow as power laws of time, with exponents which depend on the values of β and z . Previous attempts to predict the sample-to-sample fluctuations of global variables have been made in the past. For example, the center-of-mass displacement was predicted to grow as $t^{1/6}$ in KPZ clusters [17], as we confirm here for some additional examples. Moreover, we will also describe the correlation between these global magnitudes and their full histograms, which in some cases is Gaussian, and for R_{cm}^2 we will show that it corresponds to a χ^2 -distribution. The case of the squared global roughness W^2 , which has been extensively studied for globally flat interfaces [8,12,13], is more involved, but seems to share some similarities with its flat counterpart.

We will apply our scaling estimates to simulations of growing planar clusters generated by different physical systems, whose interfaces (boundaries) are known to follow FV scaling. We will start by discussing neighborhoods (balls) in the *first-passage percolation* (FPP) model, whose boundaries present 1D KPZ universality in the asymptotic regime

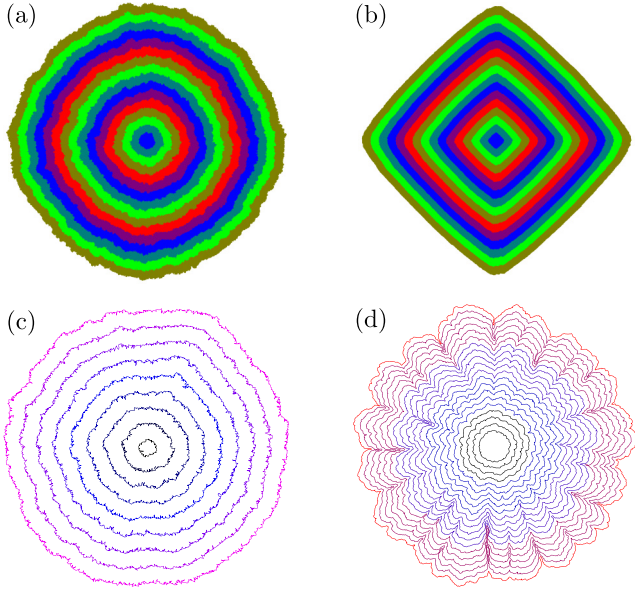


FIG. 1. Typical profiles for the different physical examples considered in this article (see definitions in Sec. III). In all cases, different colors represent different growth times. (a) FPP ball with $d_c = 1$, (b) FPP ball with $d_c = 20$, (c) isochrone curves in the random-metrics problem, (d) consecutive snapshots of the time evolution of the interface in the shadowing model of bacterial colony growth.

[4,18] if discrete lattice effects are suitably taken into account [19]. Typical FPP balls are shown in Figs. 1(a) and 1(b), depending on the level of disorder. The continuous analog of FPP is called the *random-metric problem*, where we consider isochrone curves on a two-dimensional manifold with a random (disordered) metric field which is flat on average, with only short-range correlations [3]. Typical isochrones are shown in Fig. 1(c). Interestingly, different types of one-point and two-point correlation functions are obtained depending on whether the underlying manifold is a plane, a cone, or a cylinder [20], although all these cases belong to the 1D KPZ universality class.

Additional interesting examples of rough interfaces with overall circular geometry are provided by the fronts of growing bacterial colonies [21], for which the most relevant physical parameters are the motility and the nutrient concentration. For many values of these parameters, 1D KPZ scaling can be observed, but other behaviors are also possible. Specifically, for low motility and low nutrient concentration, *shadowing effects*—whereby the growth rate at each interface point depends on the angle under which the exterior of the cluster can be seen [5]—dominate the interfacial dynamics. In Fig. 1(d), we show a typical time evolution for an interface described by this shadowing model.

This article is organized as follows. In Sec. II, we discuss our theoretical framework in order to determine the scaling exponents for global magnitudes of clusters following FV scaling. Our predictions are then tested on FPP clusters, random-metrics isochrones, and bacterial colonies in Sec. III. Additional results for the histograms and the correlations between magnitudes are reported in Sec. IV. The article ends

with a summary of our conclusions and some proposals for further work.

II. FLUCTUATIONS OF GLOBAL GEOMETRICAL OBSERVABLES

Let us consider a growing planar cluster whose boundary is described by a polar curve advancing in time, $r(\theta, t)$, subject to a stochastic evolution law which we may assume (along with the initial condition) to be isotropic. Let us also consider a local observable u which is a function of r , of $r' \equiv dr/d\theta$, and of θ itself, which we will denote by $u[r(\theta), r'(\theta), \theta]$ or just $u(\theta)$ for short when it is convenient. Its two-point correlation function can be defined as

$$C_u(\hat{\theta}) \equiv \langle u(\theta)u(\theta + \hat{\theta}) \rangle - \langle u(\theta) \rangle \langle u(\theta + \hat{\theta}) \rangle, \quad (1)$$

where we will denote the angular distance between the two points by $\hat{\theta}$. In the asymptotic regime, we assume the following scaling form for the correlation function:

$$C_u(\hat{\theta}) \approx A_u t^{2\phi_u} g_2(B_u t^{1-\zeta} \hat{\theta}), \quad (2)$$

where ϕ_u is the corresponding scaling exponent, A_u and B_u are constants, $\zeta = 1/z$ is the inverse of the dynamical exponent, and $g_2(x)$ is a continuous function such that $g(x) \sim 1$ for $x \ll 1$, and $g(x) \rightarrow 0$ sufficiently fast for $x \rightarrow \infty$.

The reason behind the form of Eq. (2) is as follows. Assuming that the expected value of the radius grows as $\langle r \rangle \sim t$ and that the correlation length grows as $\xi \sim t^\zeta$, as is the case in the Family-Vicsek ansatz [7], then the angular aperture of each correlated patch along the front will be $\delta\theta_0 \sim t^{\zeta-1}$. Then, the argument of the $g_2(x)$ function should be $\delta\theta/\delta\theta_0$, as shown in Eq. (2).

As a first example, let us consider a cluster family corresponding to the KPZ universality class [9] and the local observable $u = r$. In that case, we have $\phi_u = \beta = 1/3$, and $C_r(\hat{\theta}) \sim t^{2\beta} g_2(B_r t^{1-\zeta} \hat{\theta})$, where $\zeta = 1/z = 2/3$. Assuming that our cluster ensemble possesses a well-defined correlation length, it seems appropriate to assume that all scaling observables will present a similar structure in their correlation functions.

Let us now consider the statistical distribution of the values of a *global* measure of geometric origin, such as the *area* or the *length*, which can be written as

$$U = \int_0^{2\pi} d\theta u(r, r', \theta). \quad (3)$$

This work is devoted to evaluating the sample-to-sample fluctuations of any global measure U , which will be quantified through their deviation ΔU or their variance,

$$\text{Var}(U) \equiv (\Delta U)^2 \equiv \langle U^2 \rangle - \langle U \rangle^2. \quad (4)$$

The first two moments can be written as

$$\begin{aligned} \langle U \rangle &= \int_0^{2\pi} d\theta \langle u(\theta) \rangle, \\ \langle U^2 \rangle &= \int_0^{2\pi} d\theta \int_0^{2\pi} d\theta' \langle u(\theta)u(\theta') \rangle, \end{aligned} \quad (5)$$

thus allowing us to use a more compact notation for the variance of U ,

$$\begin{aligned}\text{Var}(U) &= \int d\theta d\theta' \langle u(\theta)u(\theta') \rangle - \langle u(\theta) \rangle \langle u(\theta') \rangle \\ &= \int d\theta d\theta' C_u(\theta - \theta'),\end{aligned}\quad (6)$$

where $C_u(\theta - \theta')$ is again the correlation function for the observable u , defined in Eq. (1). Thus, we can compute the variance of U :

$$\begin{aligned}\text{Var}(U) &= \int d\theta d\theta' C_u(\hat{\theta}) = 2\pi \int_0^{2\pi} d\hat{\theta} C_u(\hat{\theta}) \\ &= 2\pi A_u t^{2\phi_u} \int_0^{2\pi} d\hat{\theta} g_2(B_u t^{1-\zeta} \hat{\theta}) \\ &\approx \frac{2\pi A_u}{B_u} t^{2\phi_u+\zeta-1} \int_0^\infty dx g_2(x).\end{aligned}\quad (7)$$

Assuming that $g_2(x)$ decays fast enough for large values of its argument, the last integral is finite and does not affect the scaling behavior, thus leading to an estimate for the sample-to-sample deviation of U ,

$$\Delta U \sim t^{\phi_u+(\zeta-1)/2}.\quad (8)$$

This expression can be motivated in a heuristic way as follows. The variance of the average of N independent identically distributed (i.i.d.) random variables $\{u_i\}$ is $\text{Var}(\bar{u}) = \text{Var}(u)/N$. Yet, if these random variables are strongly correlated among themselves, with N_p independent groups, then it is straightforward to prove that $\text{Var}(\bar{u}) = \text{Var}(u)/N_p$. If the system radius grows approximately as t and the correlation length grows as t^ζ , then each profile possesses $N_p \sim t^{1-\zeta}$ independent patches. Therefore, the variance of a global variable U must be given by

$$\Delta U \sim \frac{\Delta u}{\sqrt{N_p}} \sim t^{\phi_u+(\zeta-1)/2},\quad (9)$$

which coincides with the result shown in Eq. (8).

The rest of this section is devoted to the theoretical analysis of the sample-to-sample fluctuations of several global geometrical observables, such as the (average) radius, area, width, center of mass position, and interfacial length.

A. Radius

As it has been discussed above, the sample-to-sample fluctuations of the average radius of the cluster,

$$R = \int_0^{2\pi} d\theta \frac{r}{2\pi},\quad (10)$$

can be obtained by applying our formalism to the observable $u(r, r', \theta) = r$, which has the associated scaling exponent $\phi_r = \beta$, thus yielding the prediction $\Delta R \sim t^{\beta+(\zeta-1)/2}$. For example, in the 1D KPZ case, $\Delta R \sim t^{1/6}$, which has been numerically verified for balls in random metrics [3].

B. Area

Let us now consider the cluster area, which is given by

$$A = \int_0^{2\pi} d\theta \frac{r^2}{2}.\quad (11)$$

Within our formalism, its sample-to-sample fluctuations can be obtained choosing $u(r, r', \theta) = r^2$. The associated scaling exponent can be found through classical uncertainty propagation, $\Delta(r^2) \sim r \Delta r \sim t^{1+\beta}$. Thus, $\Delta A \sim t^{\beta+(\zeta+1)/2}$. For 1D KPZ, our prediction is $\Delta A \sim t^{7/6}$.

C. Width

In our next example, we will consider the sample-to-sample fluctuations of the interface width, defined as

$$W^2 = \int_0^{2\pi} d\theta \frac{(r-R)^2}{2\pi},\quad (12)$$

so that the fluctuations in W^2 can be obtained using our rule. The integrand $(r-R)^2$ has fluctuations of the order of $t^{2\beta}$. Thus, its variance scales as $t^{4\beta}$, and we have

$$\text{Var}(W^2) \sim t^{4\beta-1+\zeta},\quad (13)$$

which yields $\Delta(W^2) \sim t^{2\beta-1/2+\zeta/2}$. Yet, we have $\Delta(W^2) \sim W \Delta W$ and $W \sim t^\beta$, leading us to predict

$$\Delta W \sim t^{\beta-1/2+\zeta/2}.\quad (14)$$

For example, in 1D KPZ, we have $\Delta W \sim t^{1/6}$.

D. Center-of-mass position

In the absence of fluctuations, the center of mass (CM) of a growing cluster starting out as a tiny circle must remain at the origin. But, even though the statistical properties of the cluster are isotropic, each sample presents unbalances which will give rise to fluctuations in the CM position [16,17],

$$\begin{aligned}X_{\text{cm}} &= \frac{1}{A} \int_0^{2\pi} d\theta \frac{r^3}{2} \cos(\theta), \\ Y_{\text{cm}} &= \frac{1}{A} \int_0^{2\pi} d\theta \frac{r^3}{2} \sin(\theta).\end{aligned}\quad (15)$$

Each of them presents an expectation value of zero, and a nonzero variance, which shows up in the expected value of the squared displacement,

$$R_{\text{cm}}^2 = X_{\text{cm}}^2 + Y_{\text{cm}}^2 \geq 0.\quad (16)$$

Let us evaluate the sample-to-sample fluctuations of the following associated magnitude, which neglects the explicit angular dependence:

$$U = \int_0^{2\pi} d\theta \frac{r^3}{2},\quad (17)$$

and analyze the local fluctuations of $u(r, r', \theta) = r^3/2$, i.e., $\Delta u \sim t^{2+\beta}$. Thus, we have $\text{Var}(U) \sim t^{4+2\beta+\zeta-1}$. Now, we may guess that the scaling behavior of U is the same as that for $X_{\text{cm}}A$ or $Y_{\text{cm}}A$. Thus, employing the usual uncertainty propagation techniques,

$$\Delta X_{\text{cm}} \approx \frac{\Delta U}{A} + U \frac{\Delta A}{A^2}.\quad (18)$$

Both terms scale in the same way, as $t^{\beta+(1-\zeta)/2}$. Thus,

$$R_{\text{cm}}^2 \sim t^{2\beta+\zeta-1}. \quad (19)$$

Thus, the center of mass fluctuates with the same exponent as the average radius. For 1D KPZ, this leads to $R_{\text{cm}} \sim t^{1/6}$ [17].

E. Length

The length of a cluster, L , is a different type of observable. First of all, its measure may depend on the UV cutoff if the interface presents a nontrivial fractal nature. Yet, we will assume that the interface is always smooth at the microscopic level and that the total length increases linearly in time, $L \sim t$. If the (radial) slopes are small, i.e., $r'/r \ll 1$, we may write

$$\begin{aligned} L &= \int_0^{2\pi} d\theta \sqrt{r^2 + r'^2} = \int_0^{2\pi} d\theta r \sqrt{1 + \left(\frac{r'}{r}\right)^2} \\ &\approx \int_0^{2\pi} d\theta \left(r + \frac{1}{2} \frac{r'^2}{r}\right), \end{aligned} \quad (20)$$

which forces us to consider the fluctuations of the local derivative of the radius with respect to the angle, $r'(\theta)$. In order to do that, let us consider a small angle difference $\delta\theta$ and evaluate

$$r' \approx \frac{r(\theta + \delta\theta) - r(\theta)}{\delta\theta}, \quad (21)$$

so we have

$$\begin{aligned} \text{Var}(r') &= \langle r'^2 \rangle - \langle r' \rangle^2 = \frac{2}{\delta\theta^2} [\text{Var}(r) - C_r(\delta\theta)] \\ &= \frac{2t^{2\beta}}{\delta\theta^2} [g_2(0) - g_2(t^{1-\zeta}\delta\theta)] \\ &\approx -2g_2'(0) \frac{t^{2\beta+1-\zeta}}{\delta\theta} - g_2''(0)t^{2(\beta+1-\zeta)}. \end{aligned} \quad (22)$$

The first term in Eq. (22) diverges as $\delta\theta \rightarrow 0^+$ unless we can ensure $g_2'(0) = 0$, which seems a reasonable assumption within our framework. In that case, the second term provides the complete scaling,

$$\Delta(r') \sim t^{\beta-\zeta+1}, \quad (23)$$

which becomes $\Delta(r') \sim t^{2/3}$ in the 1D KPZ case. Indeed, we have $r'/r \sim t^{-1/3}$, so this ratio becomes negligibly small for large times, as expected.

Let us provide an intuitive explanation for this scaling form. Once we have ensured that the interface is smooth, we may estimate the derivative r' by assuming that the radii will span the full range of W within each correlated patch of size ξ . Thus, we expect $\Delta(r') \sim \Delta r/\delta\theta_0 \sim W/(\xi/R) \sim t^{\beta-\zeta+1}$.

The scaling form for the slopes allows us to evaluate the sample-to-sample fluctuations of the cluster length, employing Eq. (8). Indeed,

$$\text{Var}(L) \sim t^{2(\beta-\zeta+1)} t^{\zeta-1} = t^{2\beta-\zeta+1}, \quad (24)$$

which for 1D KPZ is just $\Delta L \sim t^{1/2}$.

As a curiosity, we may define the length-to-radius ratio of any cluster family or the generalized value of $2\hat{\pi}$. Of course, this $2\hat{\pi}$ value may, in general, depend on the measurement scale if the interface is fractal, but, assuming a smooth

TABLE I. Scaling exponent values for the time evolution of the sample-to-sample average and the deviation of different global geometrical observables, as functions of the β and $\zeta = 1/z$ exponents of the corresponding universality class.

Observable	Average	Fluctuations
R	1	$\beta + (\zeta - 1)/2$
A	2	$\beta + (\zeta + 1)/2$
W	β	$\beta + (\zeta - 1)/2$
R_{cm}	$\beta + (\zeta - 1)/2$	
L	1	$\beta - (\zeta - 1)/2$

behavior below the UV cutoff, we may describe the sample-to-sample fluctuations of the $\hat{\pi}$ value for the 1D KPZ case,

$$\Delta(2\hat{\pi}) \sim \frac{\Delta L}{R} + L \frac{\Delta R}{R^2}. \quad (25)$$

The first term scales as $t^{\beta-\zeta/2-1/2}$, while the second one scales as $t^{\beta+\zeta/2-3/2}$. The first term will be dominant whenever $\zeta \leq 1$, which is the case in all the considered universality classes. Therefore, we may conjecture that

$$\Delta(2\hat{\pi}) \sim t^{\beta-\zeta/2-1/2}, \quad (26)$$

which for 1D KPZ leads to $\Delta(2\hat{\pi}) \sim t^{-1/2}$. Therefore, we see that the length-to-radius ratio of different samples will converge to a common value in the long run.

F. Summary of scaling predictions

The theoretical predictions from the scaling analysis discussed in this section are summarized in Table I, which shows the scaling exponent with time for the sample-to-sample fluctuations of each observable as functions of the β and $\zeta = 1/z$ exponents of the corresponding universality class.

Thus, the following predictions can be made:

(i) The scaling exponent values for the sample-to-sample variation of the average radius, the width, and the CM displacement coincide.

(ii) The scaling exponent for the sample-to-sample variation of the area equals the previous exponent plus one.

(iii) We may obtain both the growth and the dynamical exponents using, e.g., the fluctuations of the average radius and the interface length.

III. NUMERICAL RESULTS

In this section, we will compare our theoretical predictions, collected in Table I, with numerical simulations of different models which are known to follow FV scaling. As examples of systems in the KPZ universality class, we will discuss first-passage percolation (FPP) and random-metrics models. Both of them (with the latter in particular) happen to display the expected behavior with relative ease. As examples of non-KPZ universality classes, we will consider a shadowing model and, in Appendix A, two flavors of the random deposition model [1] for circular clusters.

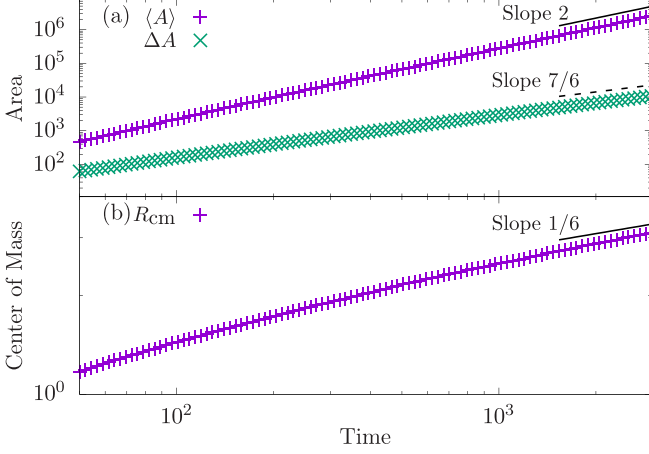


FIG. 2. Deviation of some global magnitudes for FPP isochrones with $d_c = 1$: average radius, area, and center-of-mass deviation. The straight lines in each panel represent the corresponding theoretical expectation for 1D KPZ behavior; see Table II.

A. First-passage percolation

Our first example will be first-passage percolation (FPP) on a square $L \times L$ lattice, which is defined as follows. Each lattice link k has an associated crossing time $\{t_k\}$, which are independently identically distributed (i.i.d.) random variables extracted from a certain probability distribution, with cumulative probability function $F(t)$ such that $F(0) = 0$. Employing Dijkstra's algorithm [22], we find the minimal arrival time at every vertex i starting from the lattice center [4], $\{T_i\}$. Then we determine the *ball* of radius R as the set of vertices for which $T_i \leq R$. We have chosen uniform distributions for the crossing times with mean μ and deviation σ . The balls are then characterized by the *crossover length* $d_c \equiv \mu^2/(3\sigma^2)$. In Figs. 1(a) and 1(b), we can see typical profiles using $d_c \approx 1$ and $d_c = 20$. Notice that the average shape is nearly circular in the first case and similar to a diamond in the second case. Yet, the fluctuations are known to correspond to KPZ for all values of d_c [19,23]. Note that the boundaries of the balls, which are called *isochrone curves* or *isochrones*, are not circular in average [19]. Therefore, an analysis of the width and length of the interfaces lies beyond the scope of this work.

We have run 10^4 simulations on $L = 2401$ FPP lattices, using uniform time distributions with $\mu = 5$ and different d_c . The time evolution of the average and deviation of the area and the CM displacement are shown in Fig. 2 for $d_c = 1.04$ and in Fig. 3 for $d_c = 20$. Notice that for this discrete model in particular, the aforementioned global magnitudes are easier

TABLE II. Same as Table I, but for the specific case of the 1D KPZ universality class, in which $\beta_{\text{KPZ}} = 1/3$ and $\zeta_{\text{KPZ}} = 2/3$.

Observable	Average	Fluctuations
R_{KPZ}	1	1/6
A_{KPZ}	2	7/6
W_{KPZ}	1/3	1/6
$R_{\text{cm,KPZ}}$	1/6	
L_{KPZ}	1	1/2

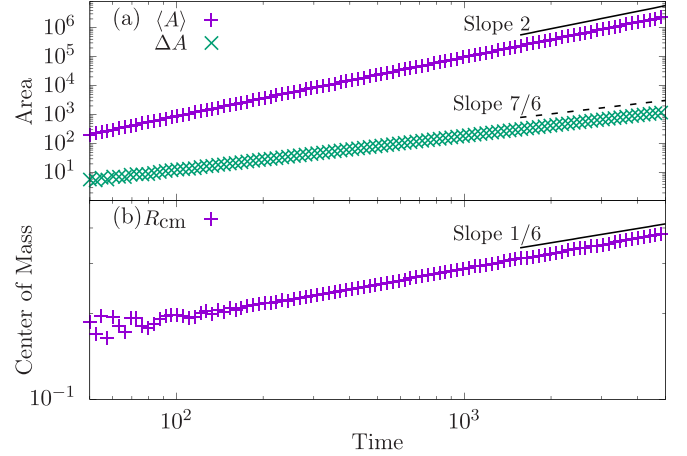


FIG. 3. Deviation of some global magnitudes for FPP isochrones with $d_c = 20$: average radius, area, and center-of-mass deviation. The straight lines in each panel represent the corresponding theoretical expectation for 1D KPZ behavior; see Table II.

to obtain because they are measured in the bulk. The solid black lines show the theoretical predictions, extracted from Table II (1D KPZ behavior), and show good agreement with the simulation data.

B. Random metrics

The FPP problem is a discrete analog of the more general *random-metrics* problem [3]. In the latter, we consider a random two-dimensional manifold, flat in average, whose metric tensor presents only short-distance correlations, and obtain the isochrone curves by integrating Huygens' equation,

$$\partial_t \vec{r} = \vec{n}_g(\vec{r}), \quad (27)$$

where $\vec{n}_g(\vec{r})$ denotes the local normal to the isochrone at position \vec{r} , according to the metric tensor g . Interestingly, both the isochrones and the times of arrival present very accurate 1D KPZ scaling from the beginning [3].

We have performed 1280 simulations of Huygens' equation, given by Eq. (27). The details regarding the simulations can be found in Appendix B. Each simulation starts out with a very small ball, with initial radius 0.05, and propagates it through a random-metric field with uniformly distributed eigenvalues $\lambda \in [1/20, 1]$, using a time step $\Delta t = 5 \times 10^{-3}$. We have obtained the full set of global observables: average radius, area, width, CM displacement, and length, whose time evolutions are shown in Fig. 4, along with the theoretical predictions extracted from Table II. Notice that in all the considered cases, the theoretical lines accurately describe the simulation data.

Furthermore, we have checked the length-to-radius ratio, i.e., the value of $2\hat{\pi}$, and the results are shown in Fig. 5. Indeed, the theoretical predictions are once more correct, with the ratio converging to a fixed value whose fluctuations decay as $t^{-1/2}$, as predicted by Eq. (26).

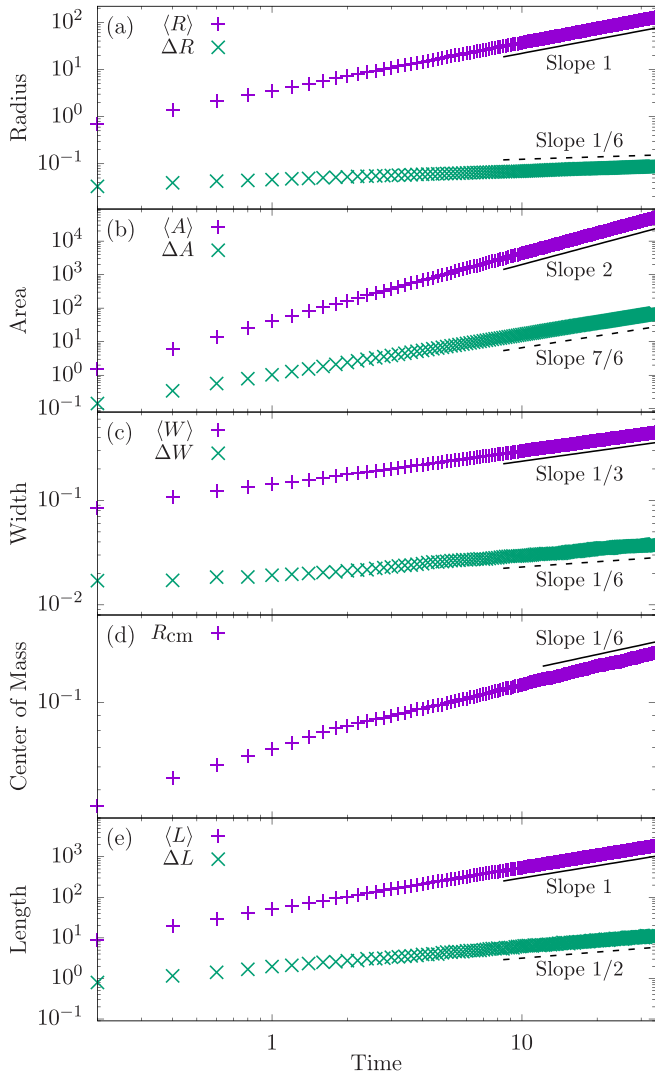


FIG. 4. Expected values and deviations for the global magnitudes for random-metric isochrones: (a) radius, (b) area, (c) width, (d) center-of-mass displacement, and (e) length. The straight lines in each panel represent the corresponding theoretical expectation for 1D KPZ behavior; see Table II.

C. Shadowing model

Motivated by the morphological instabilities of the fronts of growing planar bacterial colonies, shadowing effects may

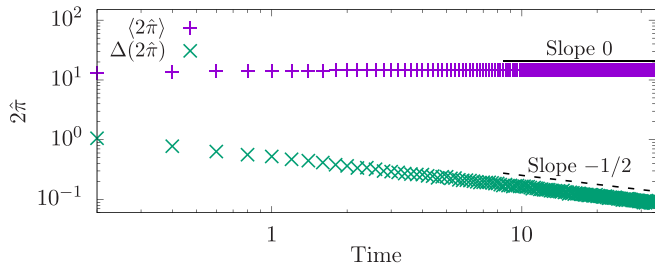


FIG. 5. Expected values and variances of the length-to-radius ratio, or $2\hat{\pi}$, for random-metric isochrones, along with the comparison to the theoretical prediction, given by Eq. (26), for 1D KPZ behavior.

be introduced phenomenologically into the radial KPZ equation, such that each point at the interface moves along the normal direction with a velocity which is proportional to the local *aperture angle*, i.e., the fraction of rays emanating from the point which does not intersect the interface [5,24]. The resulting continuum model is given by the following equation:

$$\partial_t \vec{r} = [A_0 + A_1 K(\vec{r}) + A_a \Theta_a(\vec{r}) + A_n \eta] \vec{n}, \quad (28)$$

where \vec{r} is any interface point, \vec{n} is the local exterior normal, $K(\vec{r})$ denotes the curvature of the interface at that point, $\Theta_a(\vec{r})$ is the local aperture angle, and η is a zero-average and unit variance, Gaussian, uncorrelated space-time noise. Furthermore, A_0, A_1, A_a , and A_n are positive parameters which quantify, respectively, the relative strengths of the average growth velocity of a planar front, surface tension, dependence on the aperture angle, and fluctuations. For a convex smooth shape, the aperture angle is uniformly equal to π . The subsequent dynamics tends to make peaks grow faster than valleys, thus giving rise to morphological instabilities. Indeed, in the long run, the typical cluster is composed of a set of correlated lobes separated by deep crevices whose angular distance is nearly constant in time. An example can be seen in Fig. 1(d).

We have performed 500 simulations of Eq. (28) using the same numerical scheme as in Ref. [5], for initial radius 1, $A_0 = 0, A_1 = 0.1, A_a = 1, A_n = 0.1$, and time step $\Delta t = 10^{-4}$. The technical details are discussed in Appendix B. We have measured the full set of global magnitudes: average radius, area, width, CM displacement, and length. The time evolution of their average and deviation can be found in Fig. 6. Previous work [5,24] was able to unambiguously rule out KPZ scaling for this model, even finding traces of nonuniversality both in experiments and in simulations, and very precise values of the critical exponents could not be ascertained for the FV behavior that could nevertheless be confirmed. Yet, our present global measurements agree with the scaling behavior predicted in Sec. II and summarized in Table I, but now compatible with (non-KPZ) values for the scaling exponents $\beta \approx 5/6$ and $\zeta = 1/z \approx 1/3$, implying $\alpha = \beta z \approx 5/2$.

We would like to stress that in some cases, our data show scaling ranges below one decade. A more careful analysis of the scaling exponents is provided in Appendix C, where local fits to moving time windows are employed. Yet, we would like to stress that the final aim of our numerical simulations is to check the validity of our theoretical predictions regarding the scaling exponents of the fluctuations of global geometrical magnitudes.

IV. OTHER STATISTICAL PROPERTIES

A. Histograms

We may also provide some predictions for the full histograms of some of the global observables that are considered. Indeed, if the number of patches, N_P , is large, the average radius, the area, and the length can be considered to be the sum or average of a series of i.i.d. random variables. The central limit theorem then predicts that under very broad circumstances, the probability distribution for the global observables must be Gaussian. In the random-metrics case, we have considered the full set of values of the average radius, area, and length, for a given time t , subtracted their (time-dependent)

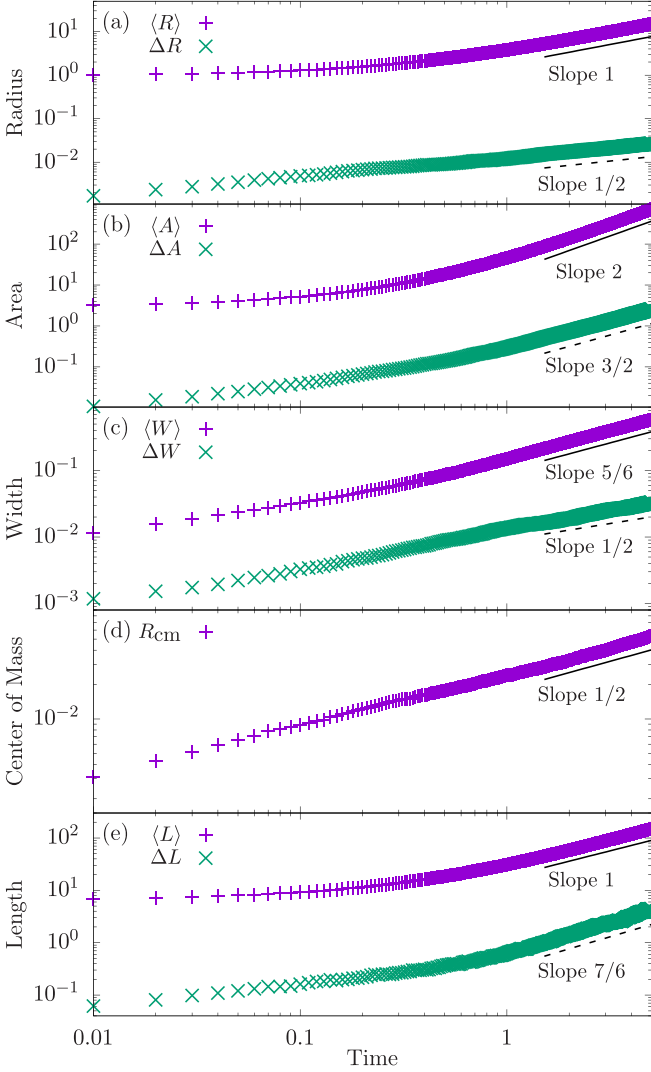


FIG. 6. Expected values and deviations for the global magnitudes for the shadowing model: (a) radius, (b) area, (c) width, (d) center-of-mass displacement, and (e) length.

average, and divided by their (time-dependent) deviation so that their average becomes zero and their variance becomes one, i.e., we have defined

$$\rho_i = \frac{U_i - \langle U(t) \rangle}{\sigma_U(t)}. \quad (29)$$

Then we have plotted the histograms of the full set of values ρ_i in Fig. 7(a), along with the unit Gaussian, showing their correspondence. The prediction is especially good for the length, with some deviation for the radius and area.

In Fig. 7(b), we show the histogram for the ρ_i values corresponding to the square of the global width, which need not be Gaussian. In fact, results associated to the KPZ class in band geometry after saturation show a very skewed histogram with a large-deviation exponential decay [8], which can be accounted for by considering the behavior of random walks [12,13]. Our case, which corresponds to circular geometry and is not saturated, also shows a large-deviation exponential decay, as we can see in Fig. 7(b).

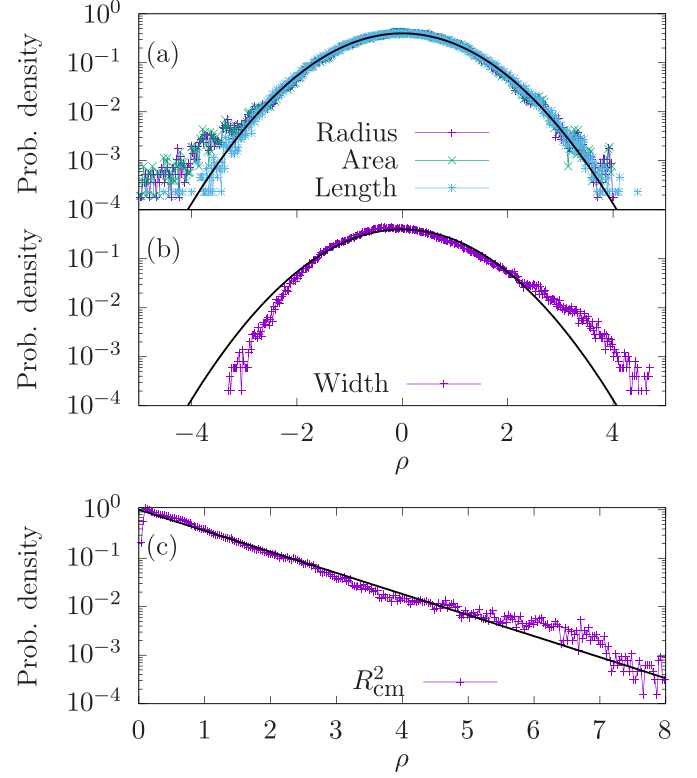


FIG. 7. Probability density for the standardized global magnitudes, given by Eq. (29), considered for the random-metrics system. (a) Radius, area, and length, along with the unit Gaussian. (b) Squared width, along with an exponential decay, as predicted in other cases in the literature [8,12]. (c) Squared CM displacement R_{cm}^2 , along with the χ^2 -distribution for $k = 2$ degrees of freedom (i.e., an exponential decay).

Furthermore, Fig. 7(c) shows the histogram for the squared CM displacements, R_{cm}^2 , merely normalized to have variance one. In this case, the theoretical prediction is not Gaussian. Indeed, $R_{cm}^2 = X_{cm}^2 + Y_{cm}^2$, where X_{cm} and Y_{cm} can be, in turn, considered to be Gaussian. Therefore, the sum of squares must follow a χ^2 -distribution for two degrees of freedom, which is an exponential distribution, as we can indeed observe in the plot.

B. Correlations between global magnitudes

It is interesting to consider whether the sample-to-sample fluctuations of different global magnitudes present correlations. Indeed, it is natural to expect that the fluctuations of the average radius and the area must be strongly correlated, with a smaller (yet positive) correlation between the CM displacement and the interface width.

In order to obtain a theoretical prediction, we consider any two global magnitudes U and V , and define their correlation coefficient,

$$r_{UV} \equiv \frac{\langle UV \rangle - \langle U \rangle \langle V \rangle}{\sigma_U \sigma_V}. \quad (30)$$

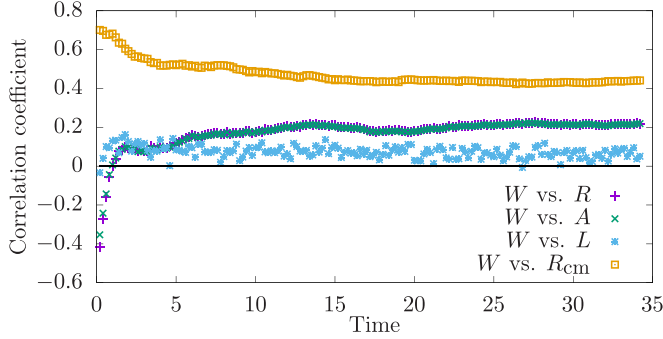


FIG. 8. Correlation coefficients, given by Eq. (30), between some pairs global magnitudes as a function of time, for the random-metrics system: width vs radius, area, length, and center-of-mass displacement.

If we assume that the correlator between different magnitudes behaves as [recall Eq. (2)]

$$C_{uv}(\theta, \theta') = A_{uv} t^{\phi_a + \phi_b} g_2(B_{uv} t^{1-\zeta} \hat{\theta}), \quad (31)$$

then

$$\begin{aligned} \langle UV \rangle - \langle U \rangle \langle V \rangle &= \int d\theta d\theta' C_{uv}(\theta, \theta') \\ &\sim \frac{2\pi A_{uv}}{B_{uv}} t^{\phi_a + \phi_b + \zeta - 1} \int_0^\infty dx g_2(x), \end{aligned} \quad (32)$$

whose time dependence is the same as that for the product $\sigma_U \sigma_V$, thus concluding that the *correlation coefficients approach time-independent values*. This is indeed what we observe in Fig. 8, where we have considered the correlation coefficients between the width and the other four global observables in the random metrics simulations. Notice that the curves for the average radius and the area overlap almost perfectly, because the correlation coefficient between them is close to one.

V. CONCLUSIONS

In this work, we have presented a scaling approach to the sample-to-sample fluctuations of global geometrical observables measured on random planar clusters whose fronts display statistical properties satisfying the Family-Vicsek ansatz. The chosen observables were the average radius, area, width, center-of-mass displacement, and length of the clusters. The sample-to-sample deviations of these observables are thus predicted to present power-law dependences with time, with exponent values that can be determined from the Family-Vicsek exponents β (growth exponent) and z (dynamical exponent).

We have tested our predictions against several different growth systems: random deposition in two different versions (see Appendix A), first-passage percolation clusters and random metrics isochrones (both belonging to the KPZ universality class), and shadowing dynamics (which does not). In all the considered cases, the predictions met the actual scaling found in the simulations.

We have also addressed the full histogram of the sample-to-sample fluctuations of these global variables. Some of them,

such as the radius, area, and length, are seen to be Gaussian. However, and in analogy to the case of KPZ growth in a band geometry [8,12,13], the histogram of the width or roughness is not Gaussian and this remains beyond our present scaling arguments. The center-of-mass displacement follows a χ^2 -distribution with $k = 2$ degrees of freedom, as predicted. Also, the sample-to-sample correlation coefficients between these magnitudes approach time-independent, limiting values, also as predicted.

In principle, our work enables alternative characterizations of the universality class in terms of exponent values, for rough interfaces with an overall, circular symmetry, by employing sample-to-sample fluctuations of global magnitudes associated to the clusters. Indeed, it is possible to obtain both the growth and the dynamical exponents using the fluctuations in two complementary global magnitudes, such as the average radius and the total length. Methodologically, this may turn out to be advantageous in the analysis of, e.g., experimental and/or simulation data.

ACKNOWLEDGMENTS

We would like to thank Pedro Córdoba-Torres, Silvio C. Ferreira, Olivier Pierre-Louis, and Kazumasa A. Takeuchi for very useful discussions. This work was partially supported by Ministerio de Ciencia e Innovación (Spain), Agencia Estatal de Investigación (AEI, Spain, Grant No. 10.13039/501100011033), and European Regional Development Fund (ERDF, A way of making Europe) through Grants No. PID2019-105182GB-I00 and No. PID2021-123969NB-I00, and by Comunidad de Madrid (Spain) under the Multiannual Agreement with UC3M in the line of Excellence of University Professors (Grants No. EPUC3M14 and No. EPUC3M23), in the context of the V Plan Regional de Investigación Científica e Innovación Tecnológica (PRICIT). I.A.D. acknowledges funding from UNED through an FPI scholarship. D.V. acknowledges funding from Ministerio de Ciencia e Innovación through FPI Scholarship No. PRE2019-088226.

APPENDIX A: RANDOM DEPOSITION

The simplest growth model is, indeed, random deposition (RD), which always yields $\beta = 1/2$ [1]. In a circular framework, we may consider two flavors of the RD class

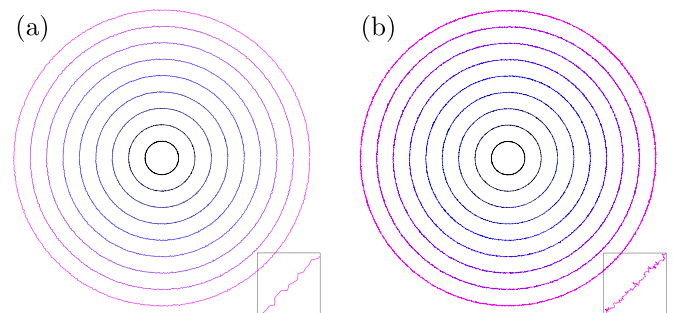


FIG. 9. Profiles for the random deposition models discussed in Appendix A: (a) Model RD-1 has a fixed angular cutoff; (b) model RD-2 has an adaptive cutoff, and thus the number of points along the interface grows with time.

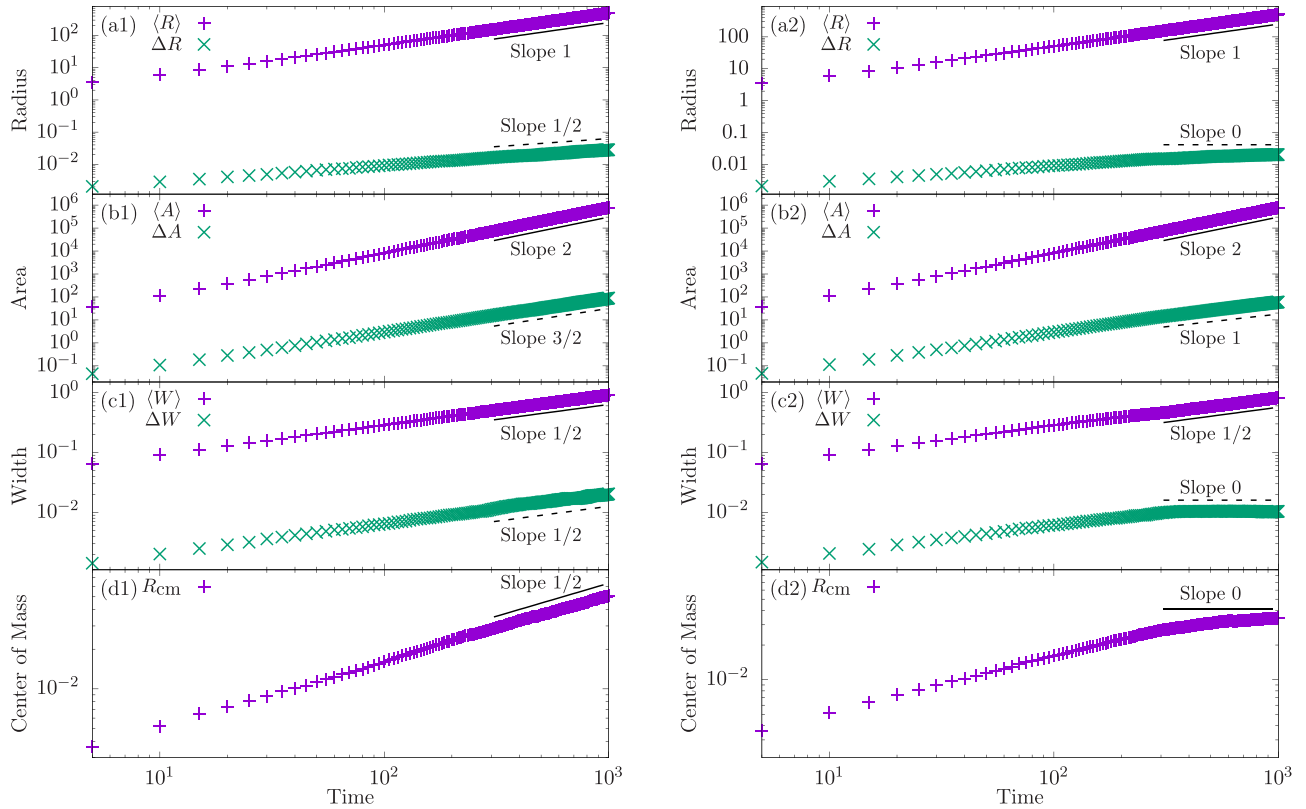


FIG. 10. Time evolution of the average and sample-to-sample deviation of global magnitudes from numerical simulations of (a1)–(d1) model RD-1 and (a2)–(d2) model RD-2. The straight lines in each panel represent the corresponding theoretical expectation; see Table III. The largest deviations between the numerical data and our scaling predictions are for (a2) the radial deviations and (d2) the CM displacement of the RD-2 model. In both cases, the expected exponent is zero, while the measured value is approximately 0.13.

(additional formulations are possible; see, e.g., [25] and related references), depending on the discretization scheme and the treatment of the UV cutoff. In what we will call model RD-1, we set up a fixed angular discretization with a UV cutoff $\Delta\theta = 2\pi/N$, where N is the number of points. Now, the interface is described by a set of N radial values, $\{r_i\}_{i=1}^N$, with $r_i = r(\theta_i)$. At each time step, we allow each r_i to grow independently of the others. In practice, we are imposing that each wedge $\Delta\theta$ remains completely correlated. Therefore, $\xi \sim t$, i.e., the correlated patches grow as fast as the interface itself and $\zeta = 1$.

Model RD-2, on the other hand, includes a UV cutoff for length instead of an angular one [3,26,27]. Therefore, the length of the correlated patches remains time independent, and $\zeta = 0$. The differences between both RD models can be seen in the profiles shown in Fig. 9.

The predictions for the sample-to-sample fluctuations of global magnitudes vary for the two models. We discard the cluster length because our calculation assumed that the interface was smooth enough at the cutoff scale, which is not the case here. The remaining scaling exponents are shown in Table III and have been measured in the numerical simulations shown in Fig. 10. In our simulations, we have run 1000 samples with a growth velocity $v = 1$, $\Delta t = 0.01$, and unit adaptive UV cutoff for the RD-2 model. The largest discrepancy between the theoretically expected exponents and those measured in the simulations is found in model RD-2 for the deviations of the average radius and for the CM deviation;

in both cases, we expect a zero exponent value, but we measure 0.13 approximately, possibly due to limitations in our longest simulation times. Other than this, the predictions seem accurate.

APPENDIX B: NUMERICAL DETAILS

This section provides further details regarding the numerical simulations discussed in the text, specifically the random metrics and the shadowing model discussed in Secs. III B and III C, respectively. Both of them are continuous models which are simulated following the adaptive and intrinsic-geometry principles discussed in [26]. Indeed, the interface is represented as a (periodic) *doubly linked list* of points on the plane in C++, which follows a resolution condition: the distance between any two neighboring points must lie in the interval

TABLE III. Scaling behavior of different geometric global observables for the RD-1 and RD-2 models. The growth exponent $\beta = 1/2$ for both models, but $\zeta = 1$ for RD-1 and $\zeta = 0$ for RD-2.

Observable	Scaling exponent	RD-1	RD-2
ΔR	$\beta + (\zeta - 1)/2$	1/2	0
ΔA	$\beta + (\zeta + 1)/2$	3/2	1
ΔW	$\beta + (\zeta - 1)/2$	1/2	0
R_{cm}	$\beta + (\zeta - 1)/2$	1/2	0

$[l_0, l_1]$. If points separate too much, a new point is created in the middle, following a suitable (usually linear) interpolation. If points approach too much, one of them is removed. This procedure requires a dynamical data structure, which is easily implemented in C++. Moreover, all operators appearing in the discretized version of the evolution equation must fulfill an intrinsic-geometry condition, i.e., they must be chart independent.

The *random-metrics* problem is thoroughly discussed in [3], and the simulation protocol is again the one discussed in [26], using adaptive cutoffs $l_0 = 0.01$ and $l_1 = 0.05$. The initial condition is a small circumference of radius $r_0 = 1$. In this case, the metric tensor at every point is simulated as a random matrix field. The metric matrix at each point is sampled in the following way. First, the two eigenvalues are selected from a uniform distribution in $[\lambda_0, \lambda_1]$, where $\lambda_0 = 0.05$ and $\lambda_1 = 1$. Then, we perform a random rotation of an angle θ uniformly sampled in $[0, 2\pi)$. In this case, the time evolution follows Huygens equation, given by Eq. (27), which is a stochastic differential equation in which the noise term is hidden in the $n_g(\vec{r})$ vector, i.e., the choice of normal to the interface at each point. In order to find this normal vector, we estimate the tangent vector to the curve as the vector joining the two nearest neighbors, and the normal vector is then obtained as perpendicular to the tangent vector according to the local metric tensor.

The *shadowing model*, which is thoroughly discussed in [5], is performed on an Euclidean plane and thus presents no subtleties related to Riemannian geometry. The evolution equation, given by Eq. (28), contains a normal growth term, a local curvature term, and a noise term, which are simulated according to the principles from [26], using adaptive cutoffs $l_0 = 0.01$ and $l_1 = 0.1$. The initial condition is a small circumference of radius $r_0 = 1$. The new term is the *shadowing term*, which links the local growth rate to the local aperture angle. We can define this local aperture angle in simple terms as the probability that a ray emanating from the interface point will touch any other point in the interface. This term is highly nonlocal and its efficient evaluation is discussed in [5].

APPENDIX C: EFFECTIVE EXPONENTS

In this Appendix, we provide further details regarding the measurements of the scaling exponents associated to the fluctuations of the global geometrical observables. Following Refs. [16,24], we have performed fits to a scaling law of the raw data over temporal windows of a fixed width, and varying the initial time. The results are shown in Fig. 11. The width of the temporal window has been fixed to $T = 4$ for the random-metrics case and to $T = 0.2$ for the shadowing case. Notice that the different windows overlap, and the initial times are separated $\Delta T = 0.2$ and $\Delta T = 0.01$, respectively.

Figure 11(a) shows the effective exponents measured as a function of time for the fluctuations of the radius, area, width, length, and center-of-mass displacement for the random-metrics problem from the data discussed in the main text, along with the theoretically predicted value. We can observe that all the exponents present small fluctuations around their theoretical value, presenting a very short transient. The

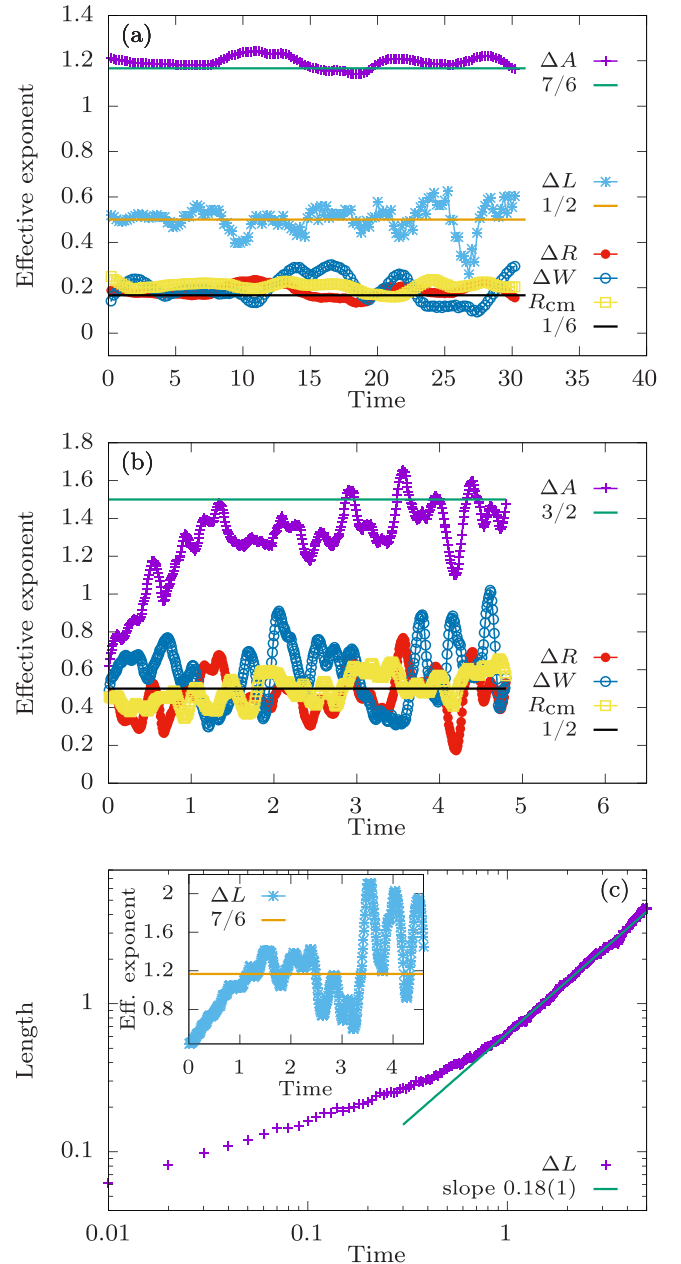


FIG. 11. Effective exponents for selected global geometric observables as a function of time for two of the models discussed in the main text. (a) The time evolution of the effective exponents for the fluctuations of the radius, area, width, and length, along with the center-of-mass displacement for the random-metrics model. The horizontal bars mark the theoretical predictions. (b) The time evolution of the effective exponents for the fluctuations of radius, area, and width, along with the center-of-mass displacement for the shadowing model, in a similar way. (c) The raw data for the length fluctuations in the shadowing model, along with the best fit. Inset: The corresponding effective exponents as a function of time.

shadowing case is subtler. Figure 11(b) presents the effective exponents measured as a function of time for the same observables, excluding the cluster length, along with our best theoretical estimate. We observe a clear transient in the effective exponent associated to the area, which is not apparent

in the other observables. The scaling exponent for the length fluctuations is detailed in Fig. 11(c), which shows the raw data, along with the best fit. The inset shows the effective exponent, along with the theoretical value, and we can observe very large fluctuations.

We should stress that our values for the scaling exponents in the random-metrics case are completely determined

from the theory, and the numerical simulations provide confirmation for their values. In the shadowing case, the scaling exponent β is obtained from the growth of the global width, thus allowing us to obtain an accurate estimate for ζ when we measure the sample-to-sample fluctuations of the global radius. The measurements of the other global exponents thus provide a consistency check for our theoretical predictions.

-
- [1] A.-L. Barabási and H. E. Stanley, *Fractal Concepts in Surface Growth* (Cambridge University Press, Cambridge, UK, 1995).
- [2] K. A. Takeuchi, M. Sano, T. Sasamoto, and H. Spohn, Growing interfaces uncover universal fluctuations behind scale invariance, *Sci. Rep.* **1**, 34 (2011).
- [3] S. N. Santalla, J. Rodríguez-Laguna, T. LaGatta, and R. Cuerno, Random geometry and the Kardar-Parisi-Zhang universality class, *New J. Phys.* **17**, 033018 (2015).
- [4] P. Córdoba-Torres, S. N. Santalla, R. Cuerno, and J. Rodríguez-Laguna, Kardar-Parisi-Zhang universality in first-passage percolation: the role of geodesic degeneracy, *J. Stat. Mech.* (2018) 063212.
- [5] S. N. Santalla, J. Rodríguez-Laguna, J. P. Abad, I. Marín, M. M. Espinosa, J. Muñoz-García, and R. Cuerno, Nonuniversality of front fluctuations for compact colonies of nonmotile bacteria, *Phys. Rev. E* **98**, 012407 (2018).
- [6] S. Najem, A. Krayem, T. Ala-Nissila, and M. Grant, Kinetic roughening of the urban skyline, *Phys. Rev. E* **101**, 050301(R) (2020).
- [7] F. Family and T. Vicsek, Scaling of the active zone in the Eden process on percolation and the ballistic deposition model, *J. Phys. A: Math. Gen.* **18**, L75 (1985).
- [8] T. Halpin-Healy and K. A. Takeuchi, A KPZ cocktail—shaken, not stirred... Toasting 30 years of kinetically roughened surfaces, *J. Stat. Phys.* **160**, 794 (2015).
- [9] M. Kardar, G. Parisi, and Y. C. Zhang, Dynamic scaling of growing interfaces, *Phys. Rev. Lett.* **56**, 889 (1986).
- [10] M. Prähofer and H. Spohn, Scale invariance of the PNG droplet and the Airy process, *J. Stat. Phys.* **108**, 1071 (2002).
- [11] I. Corwin, J. Quastel, and D. Remenik, Continuum statistics of the Airy₂ process, *Commun. Math. Phys.* **317**, 347 (2013).
- [12] G. Foltin, K. Oerding, Z. Rácz, R. L. Workman, and R. K. P. Zia, Width distribution for random-walk interfaces, *Phys. Rev. E* **50**, R639(R) (1994).
- [13] T. Antal, M. Droz, G. Györgyi, and Z. Rácz, Roughness distribution for $1/f^\alpha$ signals, *Phys. Rev. E* **65**, 046140 (2002).
- [14] C. Misbah, O. Pierre-Louis, and Y. Saito, Crystal surfaces in and out of equilibrium: A modern view, *Rev. Mod. Phys.* **82**, 981 (2010).
- [15] N. E. Muzzio, M. A. Pasquale, M. A. C. Huergo, A. E. Bolzán, P. H. González, and A. J. Arvia, Spatio-temporal morphology changes in and quenching effects on the 2D spreading dynamics of cell colonies in both plain and methylcellulose-containing culture media, *J. Biol. Phys.* **42**, 477 (2016).
- [16] S. C. Ferreira, Jr. and S. G. Alves, Pitfalls in the determination of the universality class of radial clusters, *J. Stat. Mech. Theor. Exp.* (2006) P11007.
- [17] Y. Saito, M. Duffay, and O. Pierre-Louis, Nonequilibrium cluster diffusion during growth and evaporation in two dimensions, *Phys. Rev. Lett.* **108**, 245504 (2012).
- [18] J. M. Hammersley and D. J. A. Welsh, First-passage percolation, subadditive processes, stochastic networks, and generalized renewal theory, in *Bernoulli 1713 Bayes 1763 Laplace 1813*, edited by J. Neyman and L. M. Le Cam (Springer, Berlin, Heidelberg, 1965), pp. 61–110.
- [19] I. Álvarez Domenech, J. Rodríguez-Laguna, R. Cuerno, P. Córdoba-Torres, and S. N. Santalla, Shape effects in the fluctuations of random isochrones on a square lattice, *Phys. Rev. E* **109**, 034104 (2024).
- [20] S. N. Santalla, J. Rodríguez-Laguna, A. Celi, and R. Cuerno, Topology and the Kardar-Parisi-Zhang universality class, *J. Stat. Mech.* (2017) 023201.
- [21] E. Ben-Jacob, I. Cohen, and H. Levine, Cooperative self-organization of microorganisms, *Adv. Phys.* **49**, 395 (2000).
- [22] T. H. Cormen, C. E. Leiserson, R. L. Rivest, and C. Stein, *Introduction to Algorithms* (The MIT Press, Cambridge, MA, 1990).
- [23] D. Villarrubia, I. Álvarez Domenech, S. N. Santalla, J. Rodríguez-Laguna, and P. Córdoba-Torres, First-Passage Percolation under extreme disorder: From bond-percolation to Kardar-Parisi-Zhang universality, *Phys. Rev. E* **101**, 062124 (2020).
- [24] S. N. Santalla and S. C. Ferreira, Eden model with nonlocal growth rules and kinetic roughening in biological systems, *Phys. Rev. E* **98**, 022405 (2018).
- [25] C. Escudero, Statistics of interfacial fluctuations of radially growing clusters, *Phys. Rev. E* **84**, 031131 (2011).
- [26] J. Rodríguez-Laguna, S. N. Santalla, and R. Cuerno, Intrinsic geometry approach to kinetic surface roughening, *J. Stat. Mech.* (2011) P05032.
- [27] S. N. Santalla, J. Rodríguez-Laguna, and R. Cuerno, Circular Kardar-Parisi-Zhang equation as an inflating, self-avoiding ring polymer, *Phys. Rev. E* **89**, 010401(R) (2014).